 CMES, vol.10, no.1, pp.1-12, 2005

Meshless Local Petrov-Galerkin (MLPG) Approaches for Solving Nonlinear Problems with Large Deformations and Rotations

Z. D. Han[1], A. M. Rajendran[2] and S.N. Atluri[1]

Abstract: A nonlinear formulation of the Meshless Local Petrov-Galerkin (MLPG) finite-volume mixed method is developed for the large deformation analysis of static and dynamic problems. In the present MLPG large deformation formulation, the velocity gradients are interpolated independently, to avoid the time consuming differentiations of the shape functions at all integration points. The nodal values of velocity gradients are expressed in terms of the independently interpolated nodal values of displacements (or velocities), by enforcing the compatibility conditions directly at the nodal points. For validating the present large deformation MLPG formulation, two example problems are considered: 1) large deformations and rotations of a hyper-elastic cantilever beam, and 2) impact of an elastic-plastic solid rod (cylinder) on a rigid surface (often called as the Taylor impact test). The MLPG result for the cantilever beam problem was successfully compared with results from both analytical modeling and a commercial finite element code simulation. The final shapes of the plastically deformed rod obtained from a well-known finite element code, and the present MLPG code were also successfully compared. The direct comparison of computer run times between the finite element method (FEM) and the large deformation mixed MLPG method showed that the MLPG method was relatively more efficient than the FEM, at least for the two example problems considered in the present study.

keyword: Meshless Local Petrov-Galerkin approach (MLPG), Finite Volume Methods, Mixed Methods.

1 Introduction

Accurate description and modeling of large deformations has been a very challenging problem in computational mechanics. However, during the past three decades, several researchers [Atluri (1980,1984), Belytshchko et al (1984), Malkus and Hughes(1978), Oden and Pires (1983)] have successfully developed algorithms to handle large deformations in finite element analyses. It is indeed well recognized that the FEM has certain inherent drawbacks: a) labor-intensive mesh-generation, b) shear locking, c) poor derivative solutions, and d) hourglass effects, e) mesh distortion under very large deformations, and in f) problems of strain-localization, crack-propagation, and material penetration. Eventhough ad-hoc attempts are made to alleviate some of these problems, a thorough scientific basis is still necessary. Severe localizations such as adiabatic shear banding and coalescence of microcracks can often limit the FEM solutions. The so called shock propagation based FEM codes ("Hydrocodes") provide numerical schemes that would allow the calculations to proceed smoothly through removal of highly distorted elements whose aspect ratios tend towards zero from the computations. Recently, Johnson et al (2003) proposed an "element to partcile" conversion method to alleviate the problem of highly distorted meshes in fracture and fragmentation problems. This mixed mesh/particle method seems to provide stable and useful solutions to several impact problems; howevere, these types of numerical approaches tend to remain "phenomenological" and limited to a class of problems. Ortiz and his colleagues developed FEM based fracture and fragmentation algorithms in which cohesive zones are assumed between element boundaries and cracks can be propagated between the elements using cohesive laws [Ortiz and Pandolfti (1999)]. They used advanced nonlinear error estimation and non smooth contact algorithms to assure numerical accuracy and stability. Unfortunately, this advanced FEM approach seems to suffer from mesh-influenced solutions. The problem of time consuming mesh generation process and the need for intelligent mesh design make FEM based approaches more complicated and unattractive.

[1] University of California, Irvine Center for Aerospace Research & Education
5251 California Avenue, Suite 140
Irvine, CA, 92612, USA
[2] Army Research Office, RTP, NC

In contrast, the meshless methods have become very attractive for eliminating the mesh distortion problems due to large deformations. Some meshless methods are based on the global weak forms, such as the smooth particle hydrodynamics (SPH) and the element-free Galerkin methods (EFG). They may require certain node distribution pattern or background cells for integration, which may be not satisfied while meshes are distorted during large deformations.

As a general framework for developing meshless methods, the MLPG approach provides the flexibility in choosing the local weak forms, the trial functions, and the independent test functions for solving PDEs, pioneered by Atluri and his colleagues [Atluri and Zhu(1998), and Atluri (2004)]. Some distinct advantages of the MLPG approach include: a) all weak forms are formulated locally; b) various trial and test functions can be chosen and combined together for solving one problem; c) overlapping local sub-domains can be chosen in a way to match problems and algorithms in any special cases; d) it is flexible to extend and incorporate the MLPG continuum methods with others, including molecular dynamics (MD). The MLPG approach has been used to solve various problems successfully, and has been demonstrated as to its its suitability for computational mechanics, including the work in fracture mechanics [Atluri, Kim and Cho (1999)], fluid mechanics [Lin and Atluri (2001)], and 3D elasto- statics and dynamics [Han and Atluri (2004ab)] and so on. A very comprehensive summary has been presented in the monograph by Atluri [2004].

Most recently, a new meshless mixed finite volume method has been presented by [Atluri, Han and Rajendran (2004)], in which the strains are also interpolated independently from the displacements. The key feature of this new method is to interpolate the derivatives of the primary variables independently, which makes the MLPG method computationally more efficient. The calculation of the derivatives is required at each integration point in the primal MLPG methods, which is computationally costly. With the mixed method, the strain-displacement compatibility is enforced at nodal points by using the collocation method. In addition, it requires only C0 continuities for the trial functions, instead of C1 continuities. Thus a smaller support size can be used and the number of neighboring nodes is reduced dramatically, especially for 3D cases. At the same time, it still retains the simple physical meaning as the momentum balance law of the local sub-domains, while the accuracy of the secondary variables has been improved. The mixed method has been applied to solve the elasto-static problems successfully [Atluri, Han and Rajendran (2004)].

In the present study, the mixed method is extended for the nonlinear analysis with large deformations. It is well known that the gradients of the displacements (or velocities) are widely used for the nonlinear analysis, such as the material constitutive models and the momentum balance law. The strain tensor is not enough to capture all deformation information, because the spin tensor plays an important role in the balance law, as well as the stress update [Atluri (1980)]. Therefore, the gradients of the velocities are chosen to be interpolated independently in the present study, instead of the strains. Thus the local weak forms are integrated based on the gradient interpolation, as well as the material constitutive models. As the primal variables, the velocities are chosen as the degrees of freedom for each node, and their gradients are mapped back by enforcing the compatibility conditions at nodal points through the collocation method. This special combination also demonstrates the flexibility of the general MLPG approach. The present MLPG mixed method is applied to solve some example nonlinear static and dynamic problems. An explicit algorithm is used in the present study to simulate the high-speed impact problems. The examples demonstrate the suitability of the MLPG mixed finite-volume method for nonlinear problems with large deformations and rotations.

The paper formulates the local weak forms for the nonlinear mechanics with large deformations in Section 2. It also includes the numerical implementation of the MLPG method through the mixed approach. Numerical examples are presented in Section 3, for both static and dynamic problems in 2D and 3D cases. Some conclusions and discussions are given in Section 4.

2 MLPG Mixed FVM for finite strain problems

2.1 Finite strain deformation

In the present study, we use an updated Lagrangian formulation. Let x_i be the spatial coordinates of a material particle in the current configuration. Let $\dot{S}_{ij}$ be the Truesdell stress-rate (the rate of second Piola-Kirchhoff stress as referred to the current configuration); and let $\dot{\sigma}^J_{ij}$ be the Jaumann rate of Kirchhoff stress (which is J times the Cauchy stress, where J is the ratio of volumes). It is

known [Atluri (1980)]:

$$\dot{S}_{ij} = \dot{\sigma}^J_{ij} - D_{ik}\sigma_{kj} - \sigma_{ik}D_{kj} \tag{1}$$

where D_{ij} is the symmetric part of the velocity gradient. The skew-symmetric part of the velocity gradients is denoted as W_{ij}, i.e.

$$W_{ij} = \frac{1}{2}(v_{i,j} - v_{j,i}) \tag{2}$$

Consider a body in a 3D domain Ω, with a boundary $\partial\Omega$, the rate forms of the linear and angular momentum balances are [Atluri (1980)]:

$$(\dot{S}_{ij} + \tau_{ik}v_{j,k})_{,i} + \dot{f}_j = 0 \tag{3}$$

where, in a dynamic problem, $\dot{f}_j$ are appropriately defined in terms of the rate of change of inertia forces and $(\,)_{,i} = \partial(\,)/\partial x_i$; x_i are current coordinates of a material particle. In Eq. 2.2, τ_{ij}, is the Cauchy stress in the current configuration.

Consistent theories of combined isotropic/kinematic hardening finite strain plasticity that are capable of modeling the available test data (at finite strain) are fully discussed in Im and Atluri (1984). Especially, in the case of kinematic hardening plasticity at finite strains, it is desirable [see Im and Atluri (1987), and the references cited therein] to introduce the so-called plastic spin, denoted by $\mathbf{W}^p$. As seen in Im and Atluri (1987) a combined isotropic/kinematic hardening plasticity may be characterized by the following evolution equations:

$$D^p_{ij} = f_{ij}(\sigma'_{ij}, D_{ij}, W^p_{ij}, \cdots) \tag{4}$$

$$W^p_{ij} = g_{ij}(\sigma'_{ij}, r_{ij}, \cdots) \tag{5}$$

$$r^J_{ij} = h_{ij}(D^p_{ij}, W^p_{ij}, \cdots) \tag{6}$$

and

$$\dot{\sigma}^J_{ij} = k_{ij}(D^p_{ij}, W^p_{ij}, \cdots) \tag{7}$$

Here, r_{ij} is the back-stress; $\dot{r}^J_{ij}$ the Jaumann rate of the back-stress; D^p_{ij} the plastic part of the velocity strain D_{ij}; and σ'_{ij} is the deviator of the Kirchhoff stress.

Integral representations for the combined isotropic/kinematic hardening plasticity theories of the above type have been discussed in Im and Atluri (1987b). It is noted here that $r_{ij} = 0$; $W^p_{ij} = 0$ in the case of isotropic hardening. The evolution equations for $\dot{\sigma}^J_{ij}$ is given by:

$$\begin{aligned}\dot{\sigma}^J_{ij} &\equiv \dot{\sigma}_{ij} - W_{ik}\sigma_{kj} + \sigma_{ik}W_{kj} \\ &= E_{ijkl}(D_{kl} - D^p_{kl}) - W^p_{ik}\sigma_{kj} + \sigma_{ik}W^p_{kj}\end{aligned} \tag{8}$$

2.2 Local weak form with the large deformations

In the MLPG approaches, one may write a weak form over a local sub-domain Ω_s, which may have an arbitrary shape, and contain the a point $\mathbf{x}$ in question. A generalized local weak form of the differential equation in Eq. 2.2, over a local sub-domain Ω_s, can be written as:

$$\int_{\Omega_s} [(\dot{S}_{ij} + \tau_{ik}v_{j,k})_{,i} + \dot{f}_j] w_j d\Omega = 0 \tag{9}$$

where w_j are the test functions.

By applying the divergence theorem, Eq. (9) may be rewritten in a symmetric weak form as:

$$\begin{aligned}&\int_{\partial\Omega_s} (\dot{S}_{ij} + \tau_{ik}v_{j,k}) n_i w_j d\Gamma \\ &- \int_{\Omega_s} [(\dot{S}_{ij} + \tau_{ik}v_{j,k}) w_{j,i} - \dot{f}_j w_j] d\Omega = 0\end{aligned} \tag{10}$$

One may define the rate of tractions $\dot{t}_j$ as:

$$\dot{t}_j = (\dot{S}_{ij} + \tau_{ik}v_{j,k}) n_i \tag{11}$$

where n_i are components of a unit outward normal to the boundary of the local subdomain Ω_s, in its current configuration. Thus one may rewrite the local symmetric weak form as

$$\begin{aligned}&\int_{L_s} \dot{t}_i w_i d\Gamma + \int_{\Gamma_{su}} \dot{t}_i w_i d\Gamma + \int_{\Gamma_{st}} \dot{\bar{t}}_i w_i d\Gamma \\ &- \int_{\Omega_s} [(\dot{S}_{ij} + \tau_{ik}v_{j,k}) w_{j,i} - \dot{f}_i w_i] d\Omega = 0\end{aligned} \tag{12}$$

where Γ_{su} is a part of the boundary $\partial\Omega_s$ of Ω_s, over which the essential boundary conditions are specified. In general, $\partial\Omega_s = \Gamma_s \cup L_s$, with Γ_s being a part of the local boundary located on the global boundary, and L_s is the other part of the local boundary which is inside the solution domain. $\Gamma_{su} = \Gamma_s \cap \Gamma_u$ is the intersection between the local boundary $\partial\Omega_s$ and the global displacement boundary Γ_u; $\Gamma_{st} = \Gamma_s \cap \Gamma_t$ is a part of the boundary over which the natural boundary conditions are specified.

One may use the Heaviside function as the test function in the local symmetric weak form in Eq. (12), and obtain,

$$-\int_{L_s} \dot{t}_i d\Gamma - \int_{\Gamma_{su}} \dot{t}_i d\Gamma = \int_{\Gamma_{st}} \dot{\bar{t}}_i d\Gamma + \int_{\Omega_s} \dot{f}_i d\Omega \tag{13}$$

Eq. 2.3 has the physical meaning that it represents the balance law of the local sub-domain Ω_s, as conventional finite volume methods.

2.3 Meshless interpolation for the mixed method

The MLS method of interpolation is generally considered to be one of the best schemes to interpolate random data with a reasonable accuracy, because of its completeness, robustness and continuity. With the MLS, the distribution of a function u in Ω_s can be approximated, over a number of scattered local points $\{\mathbf{x}_i\}$, $(i = 1,2,...,n)$, as,

$$u(\mathbf{x}) = \mathbf{p}^T(\mathbf{x})\mathbf{a}(\mathbf{x}) \quad \forall \mathbf{x} \in \Omega_s \tag{14}$$

where $\mathbf{p}^T(\mathbf{x}) = [p_1(\mathbf{x}), p_2(\mathbf{x}), ..., p_m(\mathbf{x})]$ is a monomial basis of order m; and $\mathbf{a}(\mathbf{x})$ is a vector containing coefficients, which are functions of the global Cartesian coordinates $[x_1, x_2, x_3]$, depending on the monomial basis. They are determined by minimizing a weighted discrete L_2 norm, defined, as:

$$J(\mathbf{x}) = \sum_{i=1}^{m} w_i(\mathbf{x})[\mathbf{p}^T(\mathbf{x}_i)\mathbf{a}(\mathbf{x}) - \hat{u}_i]^2$$

$$\equiv [\mathbf{P}\cdot\mathbf{a}(\mathbf{x}) - \hat{\mathbf{u}}]^T \mathbf{W}[\mathbf{P}\cdot\mathbf{a}(\mathbf{x}) - \hat{\mathbf{u}}] \tag{15}$$

where $w_i(\mathbf{x})$ are the weight functions and $\hat{u}_i$are the fictitious nodal values.

One may obtain the shape function as,

$$u(\mathbf{x}) = \mathbf{p}^T(\mathbf{x})\mathbf{A}^{-1}(\mathbf{x})\mathbf{B}(\mathbf{x})\hat{\mathbf{u}} \equiv \mathbf{\Phi}^T(\mathbf{x})\hat{\mathbf{u}} \quad \forall \mathbf{x} \in \partial\Omega_x \tag{16}$$

where matrices $\mathbf{A}(\mathbf{x})$ and $\mathbf{B}(\mathbf{x})$ are defined by

$$\mathbf{A}(\mathbf{x}) = \mathbf{P}^T\mathbf{W}\mathbf{P} \quad \mathbf{B}(\mathbf{x}) = \mathbf{P}^T\mathbf{W} \quad \forall \mathbf{x} \in \partial\Omega_x \tag{17}$$

The weight function in Eq. (15) defines the range of influence of node I. Normally it has a compact support. A fourth order spline weight function is used in the present study.

From the definition of the rate of tractions in Eq. (14), the integrals in the local weak form in Eq. 2.3 are based on the derivatives of the shape functions given in Eq. (16). It is well known that the calculation of the derivatives of the shape functions is computationally costly. One may following the original idea reported by [Atluri, Han, and Rajendran (2004)] and interpolate the gradients of the velocities indecently. Thus no derivatives are required to perform the local weak form integration. One may use the same shape functions in Eq. (16) for the gradient interpolation, as

$$v_{i,j}(\mathbf{x}) = \sum_{K=1}^{N} \Phi^{(K)}(\mathbf{x}) v_{i,j}^{(K)} \tag{18}$$

where $v_{i,j}^{(K)}$ are the gradients of the velocities at node K, which can be determined at the nods by enforcing the compatibility condition through the standard collocation method. The interpolation of the velocities can be also written from the same shape functions, as

$$v_i(\mathbf{x}) = \sum_{J=1}^{N} \Phi^{(J)}(\mathbf{x}) v_i^{(J)} \tag{19}$$

Thereafter, the compatibility condition is enforced at node K by differentiating the velocity fields in Eq. (19), as

$$v_{i,j}(\mathbf{x}^{(I)}) = \frac{\partial v_i}{\partial x_j}(\mathbf{x}^{(I)}) \tag{20}$$

By interpolating the gradients of the velocities, as one of the key features of the mixed method, the integrals in the local weak form involve no derivatives, i.e. the differentiation operations of the shape functions. In addition, most nonlinear constitute equations are based on the gradients, and the stress measures are transformed through the gradients. By extending the mixed method by Atluri, Han, and Rajendran (2004)[wherein strains and displacements were independently interpolated], the present mixed method[wherein the displacement gradients and displacements are independently interpolated] still holds the same advantages: a) the efficiency of the present method is improved over the traditional MLPG [primal] displacement methods; b) the requirement of the completeness and continuity of the shape functions is reduced by one-order, because the gradients are interpolated independently. Thus, lower-order polynomial terms can be used in the meshless approximations, and leads to a smaller nodal influence size to speed up the calculation of the shape functions.

2.4 Small and finite strain elasto-plasticity for velocity gradients

The analyses of small and finite strain elastoplasticity are presented, along with the detailed numerical implementations for the numerical evaluations of singular integrals. We consider a general type of elasto-plastic constitutive model, which includes the isotropic, the kinematic and the combined isotropic/kinematic hardening behavior of the solid at large strains. It is known that in a kinematic hardening large strain plasticity model, if the evolution equations for the Jaumann rates of the Kirchhoff stress and of the back-stress, respectively, are simply taken to be linear functions of the plastic component of the velocity strain, certain anomalous consequences, such as an oscillatory stress response of the material in finite simple shear, may result [Atluri (1984), Reed and Atluri (1985)]. More general evolution equations, especially to account for the noncoaxiality of the Cauchy stress and the Cauchy-like back-stress in shear and nonproportional loadings, have been attempted by Atluri (1984) and by Reed and Atluri (1985) to suppress the physically unacceptable oscillatory stress responses. Although these methods based on formal continuum mechanics were quite successful for the simple shear case, the physics and micromechanics of finite plastic flow indicate that a more consistent large strain elastoplastic constitutive law should involve an evolution equation for the plastic component of the spin tensor. Such an elastic-plastic constitutive model has been developed, for instance, in Im and Atluri (1987), which is the finite strain version of the endochronic constitutive model of Watanabe and Atluri (1986). Here, the concept of a material director triad is introduced and the relaxed intermediate configuration is chosen to be isoclinic. The plastic spin tensor is defined through internal time. Such an endochronic constitutive model (for large strain elastoplasticity) employed here, can be summarized as follows.

Let N_{ij}be the normal to the yield surface in the deviatoric Kirchhoff stress space. When the stress is on the yield surface and $N_{ij}D_{ij} \geq 0$, the process is a plastic process.

$$N_{ij} = (\tau'_{ij} - r_{ij}) / \left\| \tau'_{ij} - r_{ij} \right\| \tag{21}$$

$$\zeta = D_{ij}N_{ij}/C \tag{22}$$

$$D^p_{ij} = N_{ij}\zeta \tag{23}$$

$$W^p_{ij} = \Omega_{ij}\zeta \tag{24}$$

$$\Omega_{ij} = \{ \frac{m_1(r_{ik}\tau'_{kj} - \tau'_{ik}r_{kj})}{\tau_y^2 f^2(\zeta)}, \frac{m_2(r_{ik}r_{kl}\tau'_{lj} - \tau'_{ik}r_{kl}r_{lj})}{\tau_y^3 f^3(\zeta)}, \frac{m_3(r_{ik}\tau'_{kl}\tau'_{lj} - \tau'_{ik}\tau'_{kl}r_{lj})}{\tau_y^3 f^3(\zeta)} \} \tag{25}$$

$$(\tau'_{ij} - r_{ij})(\tau'_{ij} - r_{ij}) = \tau_y f^2(\zeta) \tag{26}$$

$$\dot{\tau}^J_{ij} = \lambda(D_{kk})\delta_{ij} + 2\mu(D_{ij} - D^p_{ij}) - W^p_{ik}\tau_{kj} + \tau_{ik}W^p_{kj} \tag{27}$$

$$\dot{r}^J_{ij} = 2\mu\rho_1 D^p_{ij} - \frac{\alpha r_{ij}(D^p_{kl}D^p_{kl})^{1/2}}{f(\zeta)} - W^p_{ik}r_{kj} + r_{ik}W^p_{kj} \tag{28}$$

where, r_{ij} is the back-stress and τ'_{ij} is the deviatoric part of Kirchhoff stress τ_{ij}. $f(\zeta)$ and r_{ij} represent the expansion and translation of von Mises type yield surface. D^p_{ij} and W^p_{ij} are the rate of plastic strain and the plastic spin, respectively. ζ represents the internal time variable. It is seen that Ω_{ij} accounts for the noncoaxiality of the tensors τ'_{ij} and r_{ij}. The coefficient C is defined as a kernel function. The reader is referred to Im and Atluri (1987) for further details of the constitutive model.

2.5 Numerical quadrature

In the present study, the integrations are performed numerically by using the conventional Gauss quadrature scheme. To improve the performance of the numerical integration, the local subdomain (i.e. a circle for 2D problems) is divided into arcs, as in Atluri, Han, and Rajendran (2004). For 3D problems, the local subdomain (i.e. a sphere) is partitioned by triangles for the surface integration [Han and Atluri (2004a)]. The same algorithms are re-used in the present study.

3 Numerical Experiments

Several nonlinear problems in 2D and 3D are solved, to illustrate the effectiveness of the present method. The first two examples studied are 2D static problems, such as the patch tests, including (i) a tensile bar, (ii) a cantilever beam under shear load. The third example is the Taylor's impact problem, for explicit dynamics.

3.1 A tensile bar

A tensile bar is analyzed as the first example. The rectangular bar is subjected to tensile deformation (in plane strain) with shear free end conditions, as shown in Figure 1. It has a length of $1.0\,m$ and a width of $0.2\,m$. The material behaviour is taken to be neo-Hookean hyperelastic. The strain energy is split into deviatoric and volumetric parts to account for the incompressibility condition as:

Figure 1 : A bar under uniform tension

$$W_0 = W_{\text{deviatoric}} + W_{\text{volumetric}}$$

$$W_{\text{deviatoric}} = C_{10}(\overline{I}_1 - 3)$$

$$W_{\text{volumetric}} = \frac{9K}{2}(J^{\frac{1}{3}} - 1)^2 \tag{29}$$

where

$$\overline{I}_1 = I_1 I_3^{-\frac{1}{3}},\ I_1 = tr(\mathbf{C})$$

$$\overline{I}_2 = I_2 \overline{I}_3^{-\frac{2}{3}},\ I_2 = \frac{1}{2}(\mathbf{C}:\mathbf{C} - I_1^2)$$

$$I_3 = \det(\mathbf{C})$$

$$J = sqrt(I_3)$$

and

$\mathbf{C} = \mathbf{F}^T \cdot \mathbf{F}$is the right Cauchy-Green deformation tensor.

In the present study, the bulk modulus is taken as $2 \times 10^7\,MPa$ and the shear modulus as $7.5 \times 10^6\,MPa$. The bar is modeled with 100 nodes as 25 nodes in 4 rows. The linear displacement fields are expected in the uniform deformations. The polynomials with first order completeness are used for the MLS approximation in the present study. Therefore, the present MLPG mixed method is expected to provide an accurate solution, in the patch test. The original MLPG mixed method passed this patch test for linear elastic problems [Atluri, Han and Rajendran (2004)].

The bar is stretched to 7 times of its original length. The numerical results obtained by using the present MLPG method are compared with the analytical solution and the FEM results, shown in Figure 2. A very good agreement is observed between these solutions.

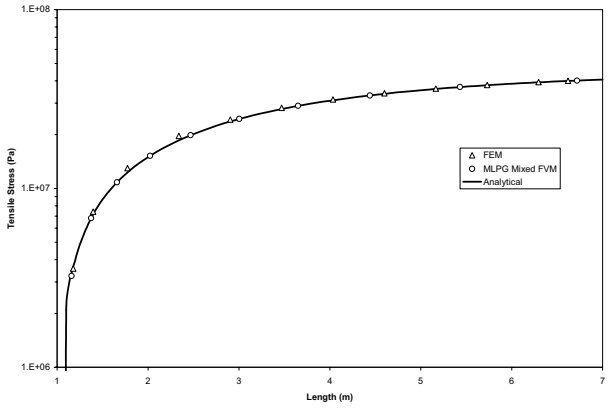

Figure 2 : Tensile stress of a bar under uniform tension

3.2 Cantilever beam

The performance of the present MLPG formulations is also evaluated, using the cantilever beam problem under a transverse load, shown in Figure 3. The beam is considered to undergo large deformations, including large strains and rotations. The linear elastic solution is given in Timoshenko and Goodier (1970), as

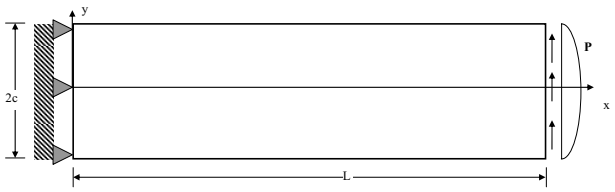

Figure 3 : A cantilever beam with an end load

$$u_x = -\frac{Py}{6\overline{E}I}\left[3x(2L-x) + (2+\overline{\upsilon})(y^2 - c^2)\right]$$

$$u_y = \frac{P}{6\overline{E}I}\left[x^2(3L-x) + 3\overline{\upsilon}(L-x)y^2 + (4+5\overline{\upsilon})c^2 x\right] \tag{30}$$

where the moment of inertia I the beam is given as,

$$I = \frac{c^3}{3} \tag{31}$$

and

$$\overline{E} = \begin{cases} E \\ E/(1-\upsilon)^2 \end{cases}$$

$$\overline{\upsilon} = \begin{cases} \upsilon & \text{for plane stress} \\ \upsilon/(1-\upsilon) & \text{for plane strain} \end{cases} \tag{32}$$

The corresponding stresses are

$$\sigma_x = -\frac{P}{I}(L-x)y$$

$$\sigma_y = 0$$

$$\sigma_{xy} = -\frac{P}{2I}(y^2 - c^2) \tag{33}$$

The problem is solved for the plane stain case with $L = 1.0$, and $c = 0.1$. The same neo-Hookean hyperelastic material is taken for the beam as it in the first example. This problem has been used as an example by Atluri, Han and Rajendran (2004) in the linear elasto-static case. The effects of the MLS support and test sizes have also been investigated. In the present study, we revisit this example with for large deformations. Based on the numerical results by Atluri, Han and Rajendran (2004), a regular uniform nodal configuration with nodal distance, d, of 0.5 is used. The number of nodes is 105. The first order MLS is used for the meshless approximation, with a support size of $1.15d$ and a test size of $0.6d$. For comparison purposes, a corresponding Quad-4 elements-based FE mesh has also been created, from the same nodes, for the FEM analysis with the commercial code MARC, .

A total transverse force of $7.58 \times 10^5 N$ is applied at the free end of the beam. There are 10 constant increment steps to solve this problem by using the present MLPG mixed method. The final vertical displacement at the free end reaches 0.83, which is more than 4 times of the height of the beam. The final deformed beam is shown in Figure 5a. The problem is also solved by using MARC, as a full nonlinear analysis. The FE results give the same deformation shown in Figure 5b. The vertical displacements are shown in Figure 6. It can be seen that the numerical results agree well with those obtained by using the FE code.

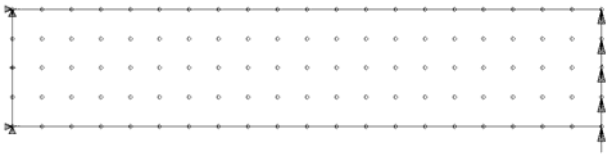

Figure 4 : Nodal configuration for a cantilever beam with 105 nodes

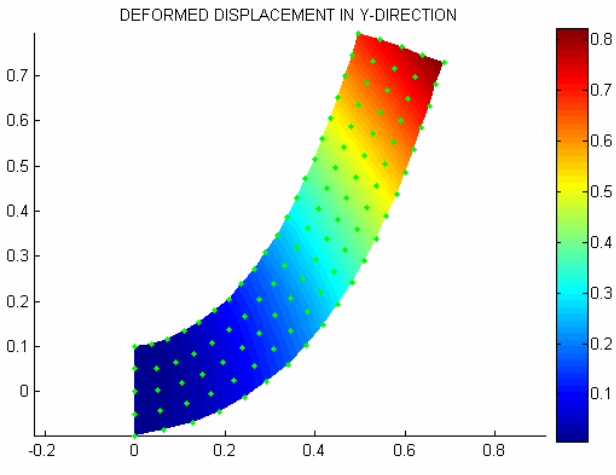

(a) The present MLPG mixed method

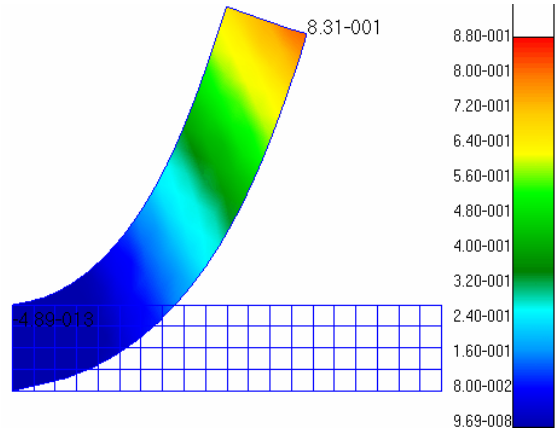

(b) FEM

Figure 5 : Vertical displacement field of the deformed cantilever beam under a transverse load.

The vertical stress distribution obtained by using the present MLPG method is shown in Figure 7a, and that

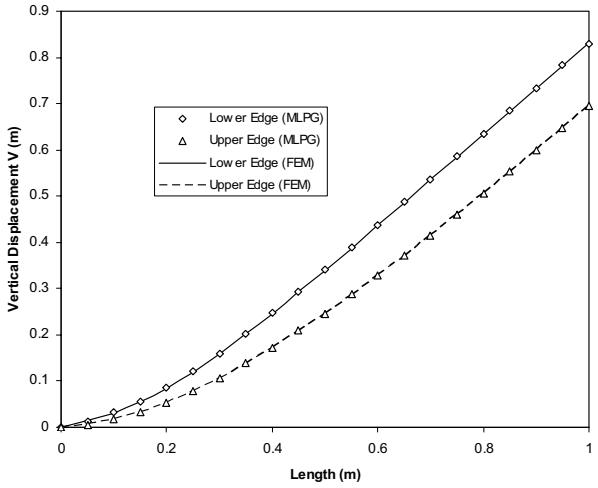

Figure 6 : Vertical displacements of a cantilever beam under a transverse load, along the lower and upper edges of the beam.

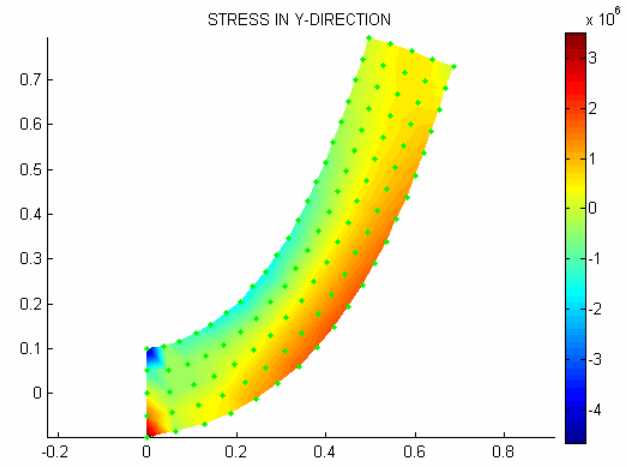

(a) The present MLPG mixed method

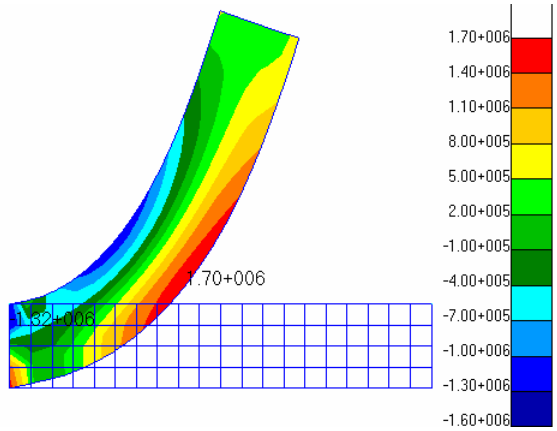

(b) FEM

Figure 7 : Stress distribution in the vertical direction of a cantilever beam under a transverse load code.

by using the FE method in Figure 7b. Both methods give the similar distributions. However, there is some difference at the corners of two ends of the beam. The stresses in the vertical direction at the lower and upper free edges are shown in Figure 8. It shows that the MLPG mixed method gives higher stresses at the fixed end, because of the stress concentration due to the fixed boundary conditions. At the free end, the MLPG mixed method gives the stress values that tend to zero as the parabolic transverse load is applied. Such numerical results confirm that the MLPG mixed method gives more accurate strain/stress (i.e. the derivative fields) results to enforce the balance laws locally. It should be pointed out that the current MLPG mixed method does not require any special numerical treatments to avoid any shear locking. It is straightforward to extend this method for other PDEs.

3.3 Taylor's problem: high speed impact

The Taylor test is often used to determine the dynamic yield stress of a material in a state of uniaxial stress. In this test, a right circular cylinder is impacted against a rigid wall. From measurements of the initial and final dimensions of the cylinder as well as the velocity of impact, the dynamic yield stress is calculated from an analytical relationship derived by Taylor (1948). However during 1990s, the Taylor test configuration has been routinely used to validate constitutive models developed for applications involving high strain rates. The high strain rate model parameters are often determined and calibrated using stress-strain curve data obtained from a number of conventional dynamic tests. Nicholas and Rajendran (1990) described these various dynamic tests and several high starin rate constitutive models. Most of the test configurations involve small strains and idealized stress / strain states, such as uni-axial stress and one-dimensional strain. The idea behind the Taylor test validation effort is to compare the high-speed-camera- measured time-resolved profiles (shapes or contours) of the plastically deforming cylinder with the profiles obtained from com-

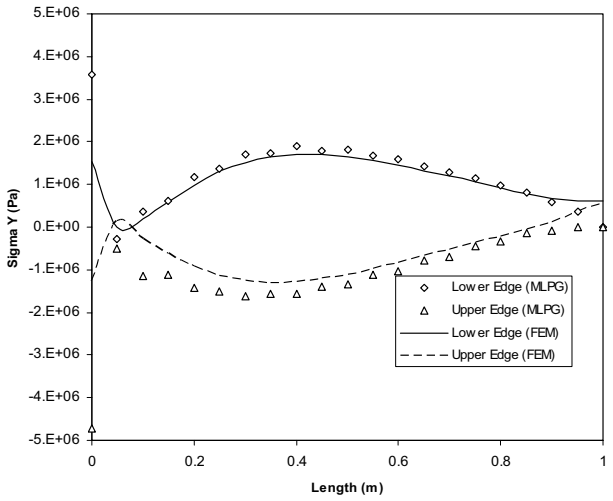

Figure 8 : Vertical stress of a cantilever beam under a transverse load, along the lower and upper edges of the beam.

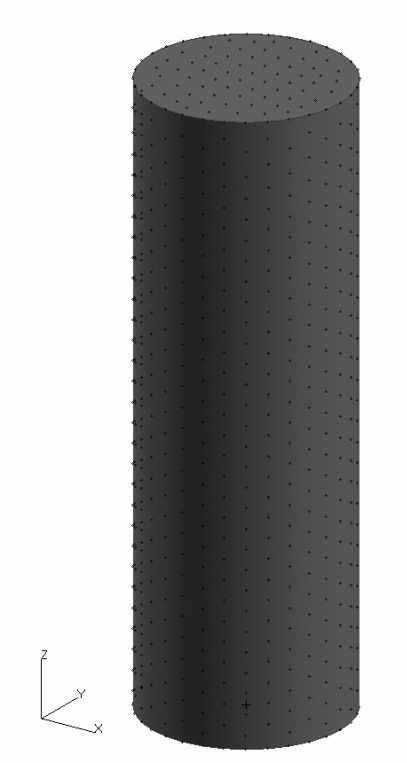

Figure 10 : A nodal configuration for the Taylor's problem: 3872 nodes.

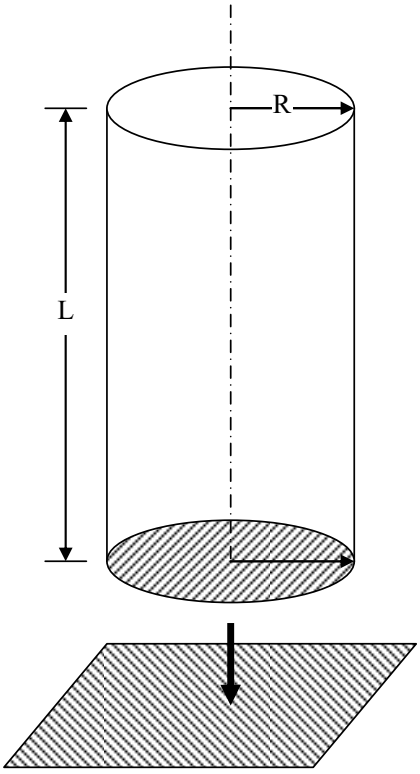

Figure 9 : Taylor's problem: a solid cylinder impacting a rigid surface

putational simulations. The loading conditions in Taylor tests involve very large deformation (>100 percent), multi-axial stress/strain state, high temperature, and very high non-uniform strain rates.

The Taylor impact problem can simply be described as a solid cylinder impacting a rigid surface in the normal direction, shown in Figure 9. In the present study, a cylinder with a length of $12.7cm$ $(0.5\,in)$ and a radius of $76.2\,cm$ $(3\,in)$ is impacting a rigid surface with an initial impact velocity of $300\,m/s$. It is assumed that there is no friction between the contact surfaces. The material is chosen as the isotropic-hardening elasto-plastic metal. The material properties are chosen as: the Young's modulus $E = 199.948\,GPa$, the Poisson's ratio $\upsilon = 0.28$, the yield strength $\sigma_s = 310.26\,MPa$, and the hardening tangent modulus $H = E/100 = 1.99948\,GPa$ for the nearly perfect plasticity. The cylinder is modeled with a nodal configuration with 3872 nodes, shown in Figure 10. There is an initial gap of $0.1mm$ between the bottom of the cylinder and rigid surface.

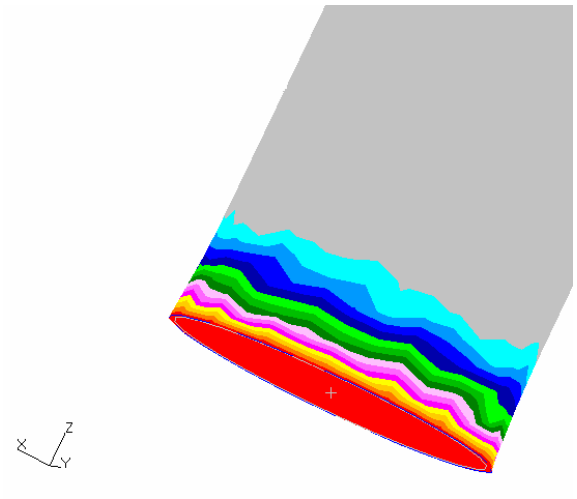

(a) MLPG Mixed Method

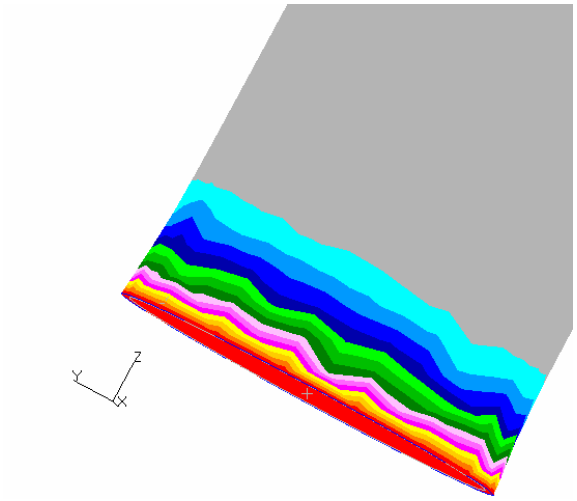

(b) Dyna3D

Figure 11 : Vertical displacement distribution of the Taylor's problem while starting contact (at t = 2 micro seconds)

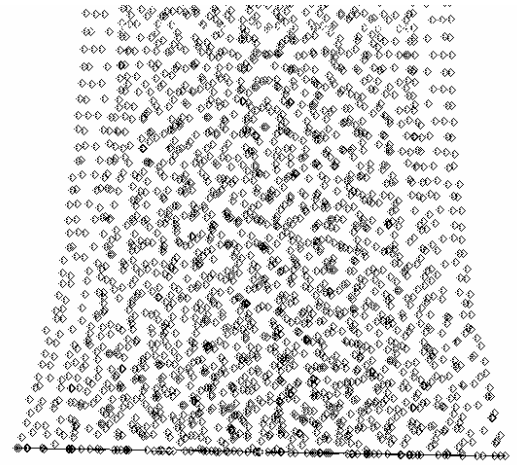

(a) MLPG Mixed Method

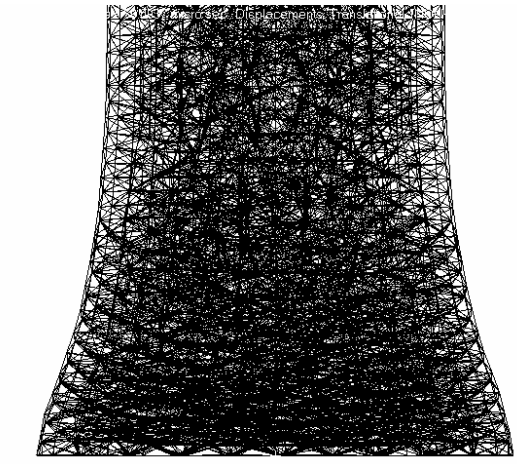

(b) Dyna3D

Figure 12 : Deformed profile of the cylinder (Taylor's problem) at t = 50 micro seconds

This Taylor impact problem is simulated using the present MLPG finite-volume mixed method, with a dynamic explicit algorithm for the direct time integration [Han and Atluri (2004b)]. The vertical displacements are shown in Figure 11a at 2 micro seconds, as the shock wave is propagating from the bottom surface towards the top surface of the cylinder. For comparison purposes, the LLNL Dyna3D (2000) is also used to analyze this problem, using the mesh generated from the same nodal configuration. Comparing Figs 11a and 11b, the wave propagation patterns from the MLPG and the Dyna3D simulations are quite similar.

The top surface of the cylinder reaches the lowest point at about 50 micro seconds. The deformed profile of the cylinder is shown in Figure 12a by using the MLPG mixed method, and in Figure 12b by using Dyna3D. Both codes give similar profiles. However, the MLPG method gives a straight corner while Dyna3D gives a curved one, for this *frictionless contact* impact. The corners of the deformed profiles are enlarged in Figure 13. After reaching the lowest point, the cylinder starts to bounce back. The

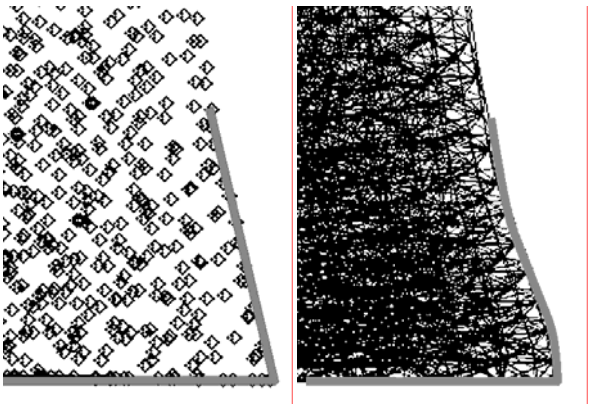

(a) the MLPG Mixed Method (b) Dyna3D

Figure 13 : The lower corner of the deformed profile of the cylinder (Taylor's problem) at t = 50 micro seconds

final deformed profiles are shown in Figure 14 at the time of 100 micro seconds. The cylinder is entirely released from contact, and bounces back at a constant velocity, in both the simulations.

In analyzing this problem, the present MLPG mixed method is used without any hour-glass control, or any other artificial numerical treatments. In contrast, one-point Gauss integration scheme is used in Dyna3D with hour-glass control. The total CPU times for the straightforward MLPG mixed method, and the Dyna3D with hour-glass control and artificial viscosity, are almost same. It clearly demonstrates the superior performance of the present MLPG mixed method as compared to the FEM methods.

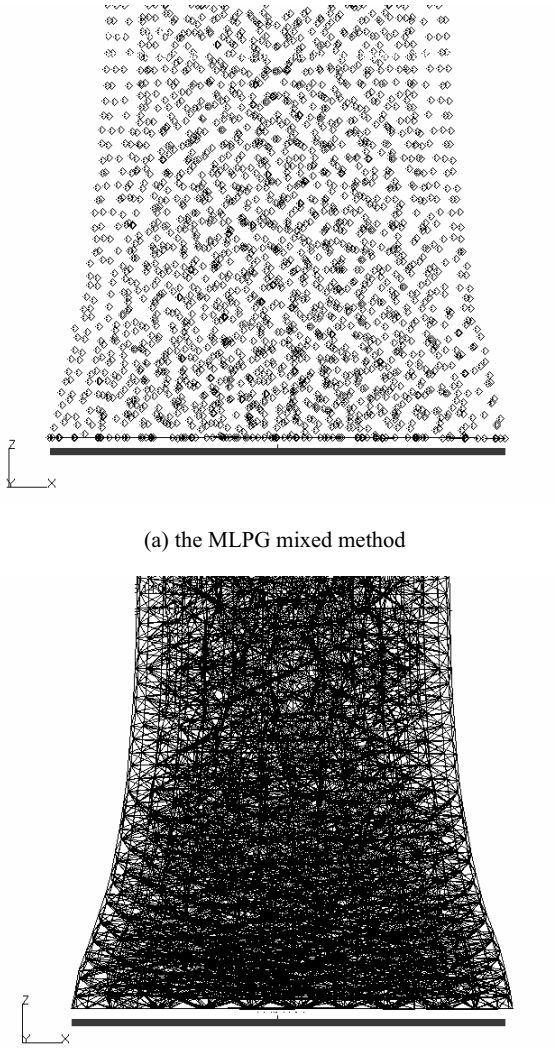

(a) the MLPG mixed method

(b) Dyna3D

Figure 14 : Spring back of the cylinder (Taylor's problem) after impact at t = 50 micro seconds

4 Closure

The mixed finite volume method (FVM) is developed for nonlinear problems, through the general MLPG approach. The MLS approximations are used for both velocity and velocity-gradients interpolations, independently. By enforcing the compatibility conditions only at nodal points, the present mixed method leads to an efficient quadrature scheme for performing the integrals in the local weak forms. The numerical examples in 2D statics show the suitability of the present MLPG mixed method for nonlinear problems with extremely large deformations and rotations. For the high-speed impact problems, the 3D Taylor-impact example demonstrates that the present mixed method possesses an excellent accuracy and efficiency, as compared to the FEM. *The present method requires no special numerical treatments to handle the nonlinear static and dynamic problems, such as the reduced integration, hour-glass control, and so on*. The present method is based on the local weak form and the nodal forces are assembled locally. It makes the present method suitable for parallel computation. With these distinct advantages, it can be concluded that the present MLPG mixed method is one of the most promising methods for the nonlinear problems with high-

speed large deformations.

Acknowledgement: The results presented in this paper were obtained during the course of investigations supported by the Army Research Office.

References

Atluri, S.N (2004): *The Meshless Local Petrov-Galerkin (MLPG) Method for Domain & Boundary Discretizations*, Tech Science Press, 665 pages.

Atluri, S. N. (1980): On some new general and complementary energy theorems for the rate problems of finite strain, classical elastoplasticity. Journal of Structure and Mechanics, vol. 8, pp. 61-92.

Atluri, S. N. (1984). On constitutive relations at finite strain hypo-elasticity and elasto-plasticity with isotropic or kinematic hardening, *Camp. Meth. Appl. Mech. Engng*, vol. 43, pp. 137-171.

Atluri, S. N.; Han, Z. D.; Rajendran, A. M. (2004): A New Implementation of the Meshless Finite Volume Method, Through the MLPG "Mixed" Approach, CMES: *Computer Modeling in Engineering & Sciences*, vol. 6, no. 6, pp. 491-514.

Atluri, S.N., Kim, H.G., Cho, J.Y. (1999): A Critical Assessment of the Truly Meshless Local Petrov Galerkin (MLPG) and Local Boundary Integral Equation (LBIE) Methods, *Computational Mechanics*, 24:(5), pp. 348-372.

Atluri, S. N.; Zhu, T. (1998): A new meshless local Petrov-Galerkin (MLPG) approach in computational mechanics. *Computational Mechanics.*, Vol. 22, pp. 117-127.

Belytschko, T.; Ong, J. S. J.; Liu, W. K.; Kennedy J. M. (1984): Hourglass Control in Linear and Nonlinear Problems, *Computer Methods in Applied Mechanics and Engineering,* Vol. 43, No. 3, pp. 251-276.

DYNA3D User Manual (1999): A Nonlinear, Explicit,Three-Dimensional Finite Element Code for Solid and Structural Mechanics, Lawrence Livermore National Laboratory.

Han. Z. D.; Atluri, S. N. (2004a): Meshless Local Petrov-Galerkin (MLPG) approaches for solving 3D Problems in elasto-statics, CMES: *Computer Modeling in Engineering & Sciences*, vol. 6 no. 2, pp. 169-188.

Han. Z. D.; Atluri, S. N. (2004b): A Meshless Local Petrov-Galerkin (MLPG) Approach for 3-Dimensional Elasto-dynamics, CMC: *Computers, Materials & Continua*, vol. 1 no. 2, pp. 129-140.

Im, S. and Atluri, S. N. (1987). A study of two finite strain plasticity models: an internal time theory using Mandel's director concept, and a general isotropic/kinematic hardening theory. *International Journal of Plasticity*, vol. 3, pp.163-191.

Johnson, G. R.; Stryk, R. A. (2003) Conversion of 3D distorted elements into meshless particles during dynamic deformation, *International Journal of Impact Engineering*, Vol. 28, pp. 947–966.

Lin, H., Atluri, S.N. (2001): The Meshless Local Petrov-Galerkin (MLPG) Method for Solving Incompressible Navier-Stokes Equations CMES: *Computer Modeling in Engineering & Sciences*, vol. 2, no. 2, pp. 117-142.

Malkus, D. S.; Hughes, T. J. R. (1978): Mixed Finite-Element Methods – Reduced and Selective Integration Techniques – Unification of Concepts, *Computer Methods in Applied Mechanics and Engineering,* Vol. 15 No. 1, pp. 63-81.

Oden, J. T.; Pires, E. B. (1983): Nonlocal and Nonlinear Friction Laws and Variational Principles for Contact Problems in Elasticity, *Journal of Applied Mechanics,* Vol. 50, No. 1, pp.67-76.

Ortiz, M.; Pandolfti, A. (1999): Finite-Deformation Irreversible Cohesive Eelemnts for Three-Dimensional Crack-Propagation Analysis, *International Journal for Numerical Methods in Engineering*, Vol. 44, pp. 1267-1282.

Reed, K. W. and Atluri, S. N. (1985). Constitutive modeling and computational implementation for finite strain plasticity. *International Journal of Plasticity*, vol. 1, pp. 63∼87.

Taylor, G.I. (1948) The use of flat-ended projectiles for determining dynamic yield stress. Proc. Roy. Soc. Lond., A, 194, pp. 289-299.

Timoshenko, S. P.; Goodier, J. N. (1976): Theory of Elasticity, 3^{rd} edition, McGraw Hill.

Watanabe, O. and Atluri, S. N. (1986). Internal time, general internal variable, and multiyield surface theories of plasticity and creep: a unification of concepts. *International Journal of Plasticity*, vol. 2, pp.107-134.